Science of the Total Environment 409 (2011) 4596–4605

Contents lists available at ScienceDirect

Science of the Total Environment

journal homepage: www.elsevier.com/locate/scitotenv

Modelling transport and transformation of mercury fractions in heavily contaminated mountain streams by coupling a GIS-based hydrological model with a mercury chemistry model

Yan Lin [a,b,*], Thorjørn Larssen [a,b], Rolf D. Vogt [a], Xinbin Feng [c], Hua Zhang [c]

[a] Department of Chemistry, University of Oslo, POB 1033, 0315 Oslo, Norway
[b] Norwegian Institute for Water Research, Gaustadalleen 21, 0349 Oslo, Norway
[c] State Key Laboratory of Environmental Geochemistry, Institute of Geochemistry, Chinese Academy of Sciences, 550002 Guiyang, China

ARTICLE INFO

Article history:
Received 9 November 2010
Received in revised form 13 July 2011
Accepted 15 July 2011

Keywords:
Hg
Modelling
GIS
HEC-HMS
WASP
Particle transport
Fluvial stream

ABSTRACT

Many heavily polluted areas are located in remote regions that lack routine hydrologic monitoring. A modelling method that can produce scenarios of water chemistry trends for regions that lack hydrological data is therefore needed. The Wanshan mining area, in Guizhou province in south-western China, is such a region, as it is heavily polluted with mercury (Hg). In order to model Hg transport in a stream draining the Wanshan mining area, a Geographic Information System (GIS) hydrologic model (HEC-HMS) was coupled with a simulation model for Hg fractions in water (WASP Hg). Hydrological variations in the stream flow can thereby be simulated based on readily available precipitation data. The WASP 7 MERC Hg model was used for simulating variations in total Hg, dissolved Hg and methyl-Hg concentrations.

The results of HEC-HMS modelling of flow show clear seasonal variation. Winter (Oct–Dec) constitutes the dry season with low flow, while the summer season (Jun–Aug) is rainy with high flow. 48% of total annual precipitation happens in the three summer months. The stream flows at the high flow events were several times higher than normal flow. The modelled total suspended solids and Hg concentrations were tested against monitoring data from two sampling campaigns conducted in September 2007 and August 2008. The model produced reasonable simulations for TSS, THg, DHg and MeHg, with relative errors generally around 10% for the modelled parameters. High flow events are the main contributors for release of both suspended particles and Hg. The three high flow events account for about 50% of annual discharge of THg. The annual total discharge of Hg was 8.8 kg Hg high up in the stream and 2.6 kg where the stream meets a large river 20 km downstream of the pollution source. Hence, about 70% of Hg is retained in the stream through sedimentation.

1. Introduction

Many mercury (Hg) mines are located in remote regions without routine hydrologic monitoring. This represents a serious obstacle for Hg modelling, as quality hydrological response data are a prerequisite for the modelling of Hg transport and fate. This study attempts to address this problem by coupling a GIS hydrologic modelling tool with a Hg transformation model. The missing hydrological data can thereby be modelled based on precipitation data linked to topographic information using the GIS hydrologic modelling tool. While discharge data are scarce, precipitation data from meteorological stations are readily available worldwide. The output of the GIS hydrologic modelling tool can then be used as input for the Hg transformation model. This method has the potential to resolve the problem of poor hydrologic data in remote or small river systems that suffer local Hg pollution.

Wanshan in Guizhou province, in south-western China, was selected as a case study area. Wanshan used to comprise the largest conglomeration of Hg mines and refining plants in China. Today, the Xiaxi River draining the Hg mining area in Wanshan is contaminated by Hg seeping out of numerous tailings. These hotspots of contamination contain mainly gangues which are mining by-product, low grade ores, that are not suitable for smelting or calcines that are generated from Hg retorting process. Hg in gangue exists mainly as cinnabar while in calcines a large part of Hg is present in elemental form. Hg concentrations of up to 4.4 g kg^{-1} have been found in these tailings (Qiu et al., 2005). The tailings are distributed throughout the headwater reaches of the river. Total Hg (THg) concentrations in the river water range from 4.5 to 2100 ng L^{-1} (Lin et al., 2010, Zhang et al., 2010a), while THg concentrations in the river sediments range from 1.1 to 360 mg kg^{-1} (Lin et al., 2010).

* Corresponding author at: Department of Chemistry, University of Oslo, POB 1033, 0315 Oslo, Norway. Tel.: +47 41768886.
E-mail address: yan.lin@niva.no (Y. Lin).

0048-9697/$ – see front matter © 2011 Elsevier B.V. All rights reserved.
doi:10.1016/j.scitotenv.2011.07.033

Contaminated river systems commonly convey roughly 90% of their total heavy metal load through transport of suspended particles (Gill and Bruland, 1990; Hines et al., 2000; Berzas Nevado et al., 2003; Zhang et al., 2010a). The Xiaxi River is a typical example, in that over 85% of the THg is found in the particulate fraction (Zhang et al., 2010a). Hg has a strong affinity for particulate matter commonly encountered in aquatic environments (Ullrich et al., 2001). The role of suspended particle transport in rivers is therefore of great importance in terms of Hg transport. The ability of river water to carry suspended particles is largely dependent on the flow velocity. Fluctuations in flow conditions affect the particle load and thus govern the concentration and transport of THg. Accurate simulation of hydrology and its relationship with particle load is therefore a necessary prerequisite for modelling Hg transport.

In freshwater systems, the organic Hg fraction mainly consists of methyl-Hg (MeHg) (Ullrich et al., 2001). Bottom sediments favour the required anoxic conditions and access to organic material for methylation (Matilainen, 1995; Watras et al., 1995a). Fluvial systems consist inherently of mainly oxic waters; therefore in this study, only the bottom sediments are considered as sites for Hg methylation. There are strong indications that methylation rates increase with decreasing pH (Xun et al., 1987; Watras et al., 1995b). The alkaline nature of the studied system (pH 7–8) may therefore also limit MeHg production. The ratio of MeHg to THg at Wanshan remains less than 5% for most of the river water samples; MeHg concentrations ranges from <0.035–11 ng L^{-1} (mean value 1.02 ng L^{-1}), with highest the concentrations found from leachate of calcine tailings (Zhang et al., 2010b).

Prediction of future Hg trends is necessary to provide information required for pollution control and remediation activities. This requires conceptually based models of Hg transport. The present study represents an effort to predict the transport and fate of Hg fractions in a network of low-order streams that lack adequate hydrological data with a combination of a hydrological GIS model and a water quality simulation model. A subroutine within the Water Quality Analysis Simulation Program (WASP) (Ambrose et al., 1988) that specifically computes Hg speciation reactions is applied to simulate concentrations of Hg fractions. The main object of this study is to set up a model process with few observational data requirements to simulate Hg transport.

2. Materials and methods

2.1. Model description

Fig. 1 shows an overview of the modelling processes using HEC-HMS. It has been shown to be a useful tool for predicting watershed runoffs (Anderson et al., 2002; Yusop et al., 2007). The Geospatial Hydrologic Modelling Extension (HEC-GeoHMS) uses ArcGIS Desktop and the Spatial Analyst extension to develop a number of hydrologic modelling inputs for the Hydrologic Engineering Center's Hydrologic Modelling System (HEC-HMS). By analysing the watershed's digital elevation model (DEM), the HEC-GeoHMS model transforms the drainage paths and watershed boundaries into a hydrologic data structure that represents the drainage network. Once the drainage network and watersheds had been determined, the Hydrologic Modelling System (HEC-HMS) was applied to simulate the watershed's precipitation-runoff processes. Hydrographs produced by the HEC-HMS model were subsequently used as hydrological input data for the Hg transport modelling.

WASP is the US EPA Water Quality Analysis Simulation Program (current version 7.3) that was developed to simulate the transport and transformation of various water body constituents (Ambrose et al., 1988). Mass balance equations account for all material entering and leaving model segments through direct and diffuse loading,

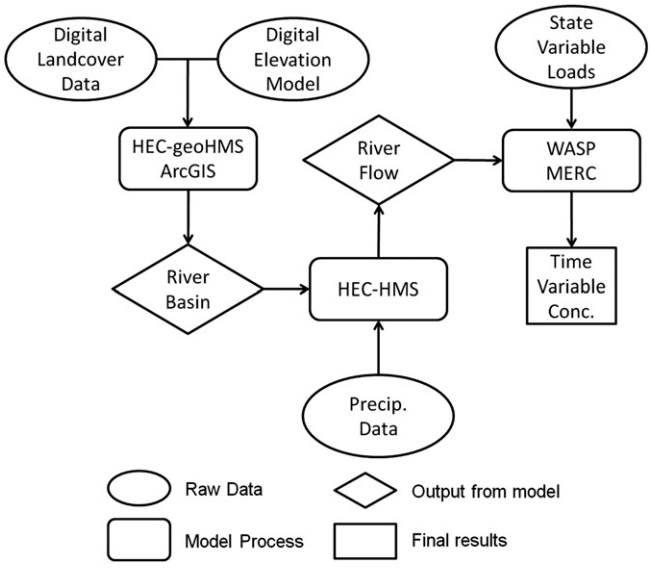

Fig. 1. Flow chart of the modelling process.

advective and dispersive transport, and any physical or chemical transformation.

WASP mercury module (MERC7) is a subroutine within WASP for Hg simulation (Ambrose et al., 1988). This module has been applied to the Carson River, Nevada, USA (Carroll et al., 2000), and the Idrija River, Slovenia (Zagar et al., 2006). It was developed to specifically compute mercury speciation and kinetic transformation. For this study, two species of mercury are modelled, inorganic mercury (Hg (II)) and MeHg. MERC7 is also capable of modelling three distinct solid types: silts and fines, sands and organic solids. Therefore, this study simulated dissolved fractions as well. Data requirements include the initial concentrations for the water column and channel bed segments, reaction coefficients for all complexation and adsorption reactions, methylation and demethylation rates and sediment diffusion rates.

2.2. Case study area

Fig. 2 shows the extent of the Xiaxi watercourse with sampling sites marked. The study area lies in Wanshan County, in the eastern part of Guizhou Province, China. Lying in the subtropical monsoon area of south-western China, the region usually experiences a long rainy period in the summer, while winter months are typically cold and dry. This seasonal rainfall frequently causes high flow rates during summer and base flow conditions during winter. As such, the hydrologic conditions of the study stream represent a typical fluvial system under the influence of a monsoon climate.

Like many other Hg mining areas, Wanshan also suffers from severe Hg pollution. After large scale Hg mining and retorting activities ceased in 2001, large amounts of gangue from the former mining and sludge from ore processing and retorting remained stockpiled. These tailings are typically located in the vicinity of headwater streams. Between 1949 and the early 1990s, approximately 130 million t of calcine was discarded, and 20 billion m^3 of Hg-containing exhaust gas was emitted (Feng and Qiu, 2008). Hg continues to leach out of the tailings and into surface runoff water, causing significant Hg contamination of downstream environments. Several studies have previously documented high concentrations of Hg in the environment in the Wanshan area (Horvat et al., 2003; Qiu et al., 2005, 2009; Lin et al., 2010).

Hg-contaminated particles are believed to enter the river from the tailings primarily during high flow events. Furthermore, Hg in the sediments associated with fine particles (such as silt and clay) are

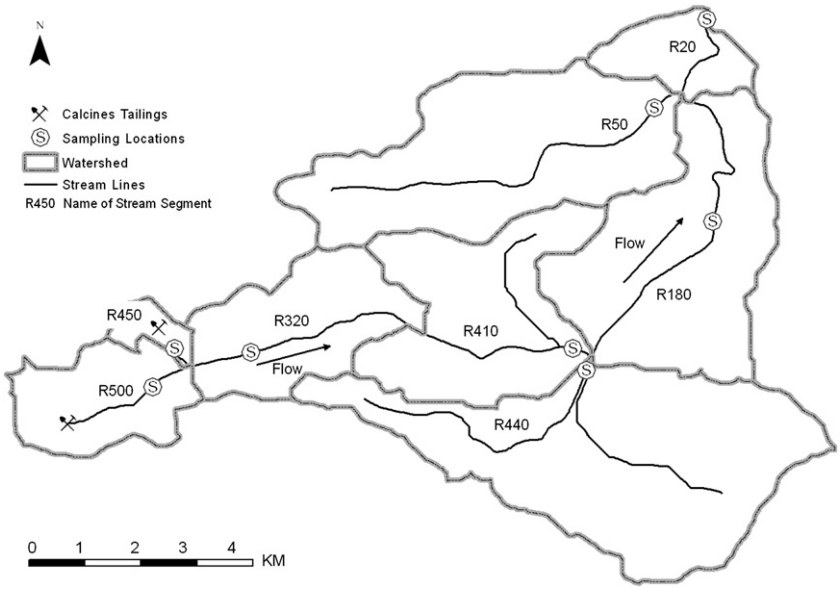

Fig. 2. Map of Xiaxi River drainage and selected sampling sites.

re-suspended and transported further downstream. Mercury also enters the water column by diffusion from the channel bed sediments. This latter source is thought to be particularly important for MeHg movement into the water column when the discharge is low.

2.3. Model parameterisation

The model optimisation was conducted on a seasonal basis. Two Hg species, divalent Hg (Hg(II)) and MeHg, were simulated. Dissolved fractions for Hg(II) were also simulated. Major model inputs are flow conditions, river geometry, contaminant loads during the modelling period and reaction coefficients. Because the study area is highly contaminated, the main Hg loading inputs are assumed to be released of tailings from Hg mining and processing. Each vertical water column is divided into two sections, a surface segment and a surface benthic segment. The whole watercourse was segregated into 8 subcatchments. The whole stream was thus divided into 8 surface segments and 8 corresponding surface benthic segments. Input data for the model, and data needed to identify the boundary conditions were taken from Zhang et al. (2010a,b) and Lin et al. (2010).

2.3.1. Flow discharge

The flow discharge in Xiaxi River was simulated from daily precipitation data, obtained from the Tongren meteorological monitoring station, roughly 20 km north of Wanshan. The geometry of each water segment is listed in Table 1. The SCS runoff curve number (CN) method (USDA, 1986) was used to simulate the runoff from each of the subcatchments, and lag time was also calculated to determine how the runoff is distributed over time. The Muskingum-Cunge routing method (Bravo et al., 1994) was used for simulating river flow in HEC-HMS.

The river channel is simplified into a trapezoid. The velocity of flow is thus calculated through the Manning formula:

$$V = \frac{1}{n} R_h^{2/3} \cdot S^{1/2}, \tag{1}$$

where

V is the cross-sectional average velocity ($m\ s^{-1}$);
n is Manning's roughness coefficient (without units; 0.035 in this case, representing earth channel — stony, cobbles);
R_h is the hydraulic radius (m), calculated according to the channel shape; and
S is the slope of the water surface (s values for each segment are listed in Table 1).

In WASP, the user should input depth (m) and velocity ($m\ s^{-1}$) as a function of flow, as shown by Eqs. (2a) and (2b):

$$V = aQ^b, \tag{2a}$$

Table 1
Geometry of Xiaxi River.

Segment no.	Segment	Length m	Slope	Bottom width m	Side slope xH:1V	Catchment area km^2	Remark
1	R450	646	0.17301	1.5	5	0.997	Source
2	R500	2675	0.04434	2	5	5.08	Source
3	R320	4687	0.02238	4	5	7.15	Main stream
4	R410	3388	0.02766	6	5	10.2	Main stream
5	R180	6813	0.01000	10	5	13.5	Main stream
6	R20	2017	0.01000	20	5	2.98	Main stream
7	R440	5688	0.03769	5	5	18.8	Tributary
8	R50	7353	0.02745	8	5	14.6	Tributary

Note: segments were illustrated in Fig. 2. R450 and R500 the place where calcine tailings are located. Slope is the segment drop to segment length ratio. Side slope is the horizontal difference to vertical difference ratio of the river bank.

and

$$D = cQ^d, \quad (2b)$$

where

Q is the flow of the segment ($m^3 s^{-1}$);
V is the velocity of the water segment under the flow of Q ($m s^{-1}$);
D is the depth of the water segment under the flow of Q (m); and
a, b, c and d are coefficients calculated fitting known V, D, and Q to Eqs. (2a) and (2b).

2.3.2. Suspended solids transport

The solubility of Hg in water is low, and Hg is highly particle affiliated in aquatic systems (Ullrich et al., 2001). Research conducted at several Hg contaminated sites show that up to 95% of THg is bound to suspended particles (Hines et al., 2000; Horvat et al., 2003; Zhang et al., 2010a). Transport by suspended solids is therefore a key factor in understanding Hg transport.

The concentrations of fine (silt and clay; diameter<0.063 mm) and coarse (sand; diameter>0.063 mm) suspended solids have been shown to have a linear correlation with flow (Carroll et al., 2000; van Rijin, 1984). During both sampling campaigns, the amount of total suspended solids (TSS) was measured gravimetrically by filtering 2 L water samples through 0.45-μm filters and then drying the filters at 103 °C–105 °C until filters reached constant weight. TSS values were tested against flow values at different locations. Due to different characteristics of tributaries flowing through calcines tailings (R450 and R500) and uncontaminated streams (R440 and R50), the linear regression was performed separately for these two categories. Fig. 3A shows the correlation between TSS and flow values at different tributaries with 95% confidential interval. A regression (Eqs. (3a) and (3b)) is thus used to define the upstream boundary conditions for TSS:

$$TSS = 25.79Q,\ R^2 = 0.89 \quad \text{(for R450 and R500)} \quad (3a)$$

$$TSS = 0.637Q,\ R^2 = 0.97 \quad \text{(for uncontaminated tributaries)} \quad (3b)$$

where

TSS is total suspended solids ($mg L^{-1}$); and
Q is the stream flow ($m^3 s^{-1}$).

Particles size distribution in water samples was analysed by Coulter Counter. Results showed that diameters of most particles were below 10 μm. Stokes' law describes how suspended solids settle from surface segments to benthic segments. The optimised Stokes settling velocities were set as 5 m day^{-1} and 25 m day^{-1} with corresponding particle diameters of 0.01 mm and 0.1 mm (fine and coarse suspended solids, respectively).

2.3.3. Hg boundary conditions

Water samples were collected at sampling stations in the water-course (Fig. 2) during moderate and high flows in September 2007 and August 2008, respectively (Zhang et al., 2010a,b). THg, dissolved Hg (DHg), methyl Hg (MeHg), reactive Hg (RHg) and TSS were analysed in all eight stream segments for the two sampling campaigns. Water samples were collected in Teflon bottles (Total Hg and MeHg). In the laboratory, water sample aliquots were filtered (0.45 μm) for determination of the dissolved fraction. Collection, storage, and preservation techniques of samples complied with US EPA Method 1631. Filters were dried to measure TSS. The Hg concentration was found to decrease rapidly downstream from the source but stabilised at 30 to 40 ng L^{-1}. The rapid decrease of Hg concentrations is likely due to high association of Hg to particles and the rapid settlement of these particles. The main source of Hg in this study was tailings with gangue and calcines (high Hg content) found at R450 and R500 (Fig. 2). THg from R450 and R500 are considered to be point sources of Hg. Carroll et al. (2000) found that stream flow had a strong relationship with THg concentrations in a gold mining area in Nevada, USA. Suchanek et al. (2009) found similar trends for creeks draining Sulphur Bank Hg Mine in California. Therefore we also apply a linear correlation with our simulated flow data with THg data to derive the Hg loading equation. THg concentrations of R450 and R500 were therefore correlated with flow values used for upstream boundary conditions, as shown in Eqs. (4a) and (4b), respectively

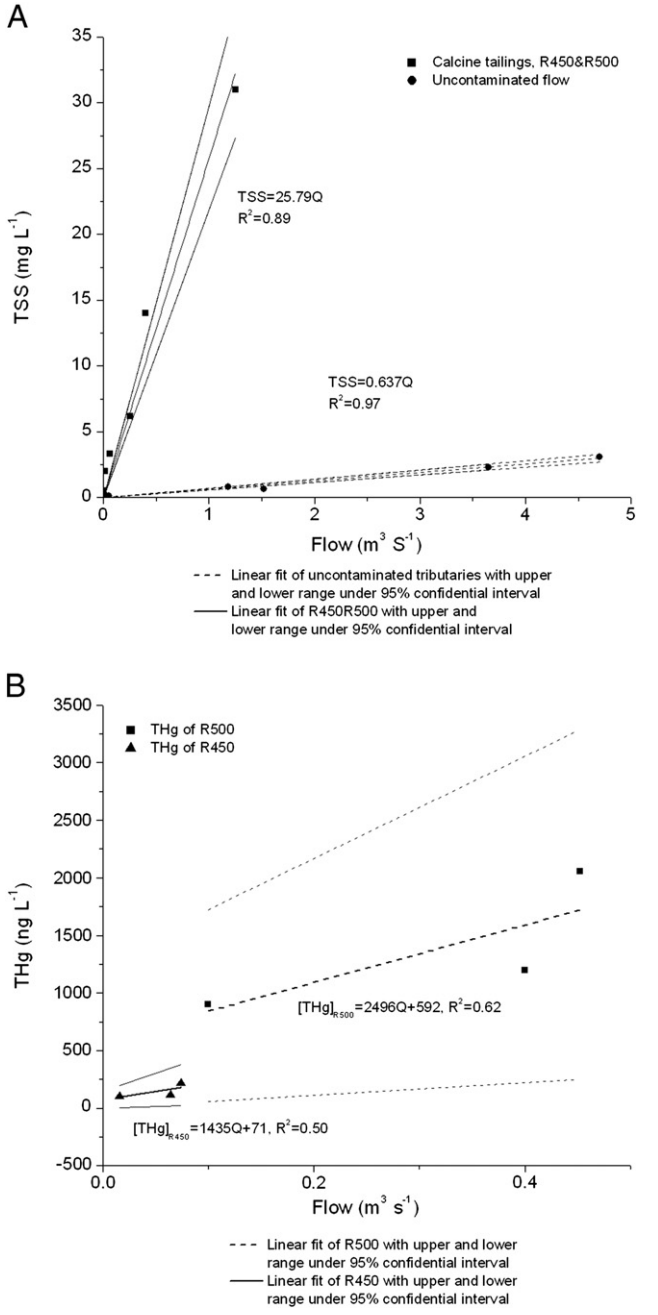

Fig. 3. Linear correlation between TSS and flow (A); linear correlation THg and flow at the R500 and R450 sites (B).

(Fig. 3B). Input values for THg concentrations were obtained from previous research at the same site (Zhang et al., 2010a,b).

$$[THg]_{R450} = 1435Q + 71,\ R^2 = 0.50 \tag{4a}$$

$$[THg]_{R500} = 2496Q + 592,\ R^2 = 0.62 \tag{4b}$$

Water column concentrations are shown in ng L^{-1}, and Q is in $m^3\ s^{-1}$. It should be noted that there were only three concentration values available in the simulation for each of the equations, as three sampling campaigns were conducted (Zhang et al., 2010a,b).

Particle-bound Hg may exist in different forms, ranging from potentially labile (as loosely sorbed to the surface of the particles) to completely inert (as grains of Cinnabar mineral). Because particle-bound Hg is by far the dominant fraction, it is important to relate how Hg is bound to the particles. A preceding study of the particulate matter in the stream sediments, using sequential extraction procedures, showed that 20–60% of the particle-bound Hg existed as highly inert residue (Lin et al., 2010). Because the study area is a former cinnabar mining area, it is reasonable to assume that these grains are weathering residues of inert HgS ore material in the carbonate gangue. Using THg as an input to the WASP model therefore presents a problem because the model is based on the assumption that all Hg is chemically available for equilibrium reactions. Instead, the chemically reactive Hg fraction (i.e., RHg) is used as input to the WASP when modelling DHg and MeHg. It must be noted that although RHg is the best available alternative data, RHg may not exactly represent the chemically reactive Hg fraction.

2.3.4. Reaction constants and partitioning coefficients

Adsorption and desorption of Hg to particles are modelled as first-order kinetic reactions according to Eq. (5). Sorption involves all of the three particle classes and both Hg(II) and MeHg:

$$K_d = \frac{\left[Hg_p\right]}{[Hg_D][Solid]} = \frac{[THg]-[Hg_D]}{[Hg_D][Solid]}, \tag{5}$$

where

K_d is the partitioning coefficient (L kg^{-1});
$[Hg_P]$ is the particulate Hg concentration (ng L^{-1}), $[Hg_P]+[Hg_D]=[THg]$, thus, $[Hg_P]=[THg]-[Hg_D]$;
$[Hg_D]$ denotes the dissolved Hg concentration (ng L^{-1}); and
[Solid] is the concentration of the solid constituent, measured as TSS (kg L^{-1}).

Methylation and de-methylation reactions occur in the channel bed sediments and are described by the first order kinetic given in Eq. (6):

$$\begin{aligned} &Methylation: \frac{\partial[MeHg]}{\partial t} = f_{temp}M[HgII] \\ &Demethylation: \frac{\partial[HgII]}{\partial t} = f_{temp}D[MeHg], \end{aligned} \tag{6}$$

where

[MeHg] is the total concentration of MeHg;
[HgII] is the total concentration of Hg(II);
t is reaction time (day);
M/D the methylation/demethylation (M/D) rate (day^{-1});
f_{temp} is a temperature factor to correct for temperatures deviating from 20 °C (dimensionless).

The temperature factor is derived by Eq. (7):

$$f_{temp} = Q_{10}^{\frac{T-20}{10}}, \tag{7}$$

where

T is the ambient temperature (°C); and
Q_{10} is a temperature coefficient, set equal to 2 as suggested in the WASP manual.

2.3.5. Model performance

Model performance was tested against concentrations of the Hg fraction that were measured during two sampling campaigns in the main stream sections (R320, R410, R180 and R20). Standard statistics of root mean squared error, relative error (%error) and bias were calculated with Eqs. (8a), (8b) and (8c), respectively:

$$Error = \left[\frac{1}{n}\sum_{i=1}^{n}\left(C_M - C_O\right)_i^2\right]^{0.5}, \tag{8a}$$

$$\%Error = 100 \cdot \left[\frac{\sum_{i=1}^{n}\left|C_M - C_O\right|_i}{\sum_{i=1}^{n}\left(C_O\right)}\right], \tag{8b}$$

and

$$Bias = \frac{\sum_{i=1}^{n}\left(C_M - C_O\right)_i}{n}, \tag{8c}$$

where

C_M is the modelled concentration (ng L^{-1}); and
C_O is observed concentration during two sampling campaign (ng L^{-1}).

2.3.6. Sensitivity analysis

In order to find the most suitable K_d value and M/D rate, a sensitivity analysis was performed using these parameters and the values resulting from the best fit between modelled and observed Hg concentrations used. This study addresses uncertainty in the estimate of DHg and MeHg as described by Eqs. (5) and (6).

Adsorption is a surface physical reaction and is therefore highly dependent on surface area available. The rate of adsorption is indirectly related to the diameter of the particles. Particle size is therefore critical, as it determines both the surface area and the Stokes' settling velocity. Due to lack of data on organic matter content for suspended particles, parameters of organic matter in the model were considered the same as those of fine particles. In the simulation of adsorption, organic matter is treated as fine particles. The minimum and maximum partitioning coefficients (K_d) for coarse particles and fine particles were established based on WASP manual (Allison and Allison, 2005). Table 2 shows the relative error for DHg results which were simulated by different K_d values for both fine and coarse particles. The most suitable partitioning coefficients for fine and coarse particles are 10^8 and 10^4 L kg^{-1} respectively.

Sensitivity analysis was also performed to determine the most suitable M/D rates. Studies by Carroll et al. (2000) and Oremland et al. (1995) have shown that methylation rates in Carson River ranged between 0.0025 and 0.011 day^{-1} and demethylation rates ranged between 0.12 and 0.55 day^{-1}. The work of Knightes et al. (2009) used 0.001 day^{-1} and 0.05 day^{-1} for methylation and demethylation rate, respectively. The WASP manual suggested values are 10^{-5}–

Table 2
Relative errors of simulated dissolved Hg for different values of K_d ($L\,kg^{-1}$) as sensitivity analysis results.

$K_d^{fine}\backslash K_d^{coarse}$	10^2	10^3	10^4	10^5	10^6
10^6	33.47	30.95	29.54	29.26	32.79
10^7	29.16	26.30	24.68	24.37	27.97
10^8	18.53	14.23	11.75	12.29	15.42
10^9	39.06	35.03	32.67	32.20	38.84

Note: K_d is the partitioning coefficient (Eq. (5)) of Hg to particles (K_d^{coarse} for coarse particles and K_d^{fine} for fine particles).

Table 3
Relative error of MeHg simulated by different M/D rates (day^{-1}) as sensitivity analysis results.

M\D	10^{-2}	10^{-1}	1
10^{-1}		28.45	25.06
10^{-2}	11.81	9.93	13.37
10^{-3}	12.20	14.14	19.53
10^{-4}	12.69	14.65	20.18
10^{-5}	14.27	16.10	20.24

Note: M stands for methylation rate; D stands for demethylation rate (Eq. (6)).

$10^{-2}\,day^{-1}$ for both methylation and demethylation (Allison and Allison, 2005). For the sensitivity analysis in this study the range of 10^{-1}–$10^{-3}\,day^{-1}$ for was used for the M/D ratio. Table 3 shows relative error for MeHg which was simulated by different M/D rates. The M/D rates that gave lowest error were found to be 0.01 and 0.1 day^{-1} for methylation and demethylation respectively.

The THg loading to system is very important. Sensitivity analysis was also carried out to access the impacts of flow on THg. A linear correlation between THg and flow was performed and Fig. 3B shows the linear correlation between THg and flow including upper and lower ranges with 95% confidential interval. The simulated THg results were tested using different regression equations within the range and Eqs. (8a), (8b), and (8c) were used to assess the range of errors.

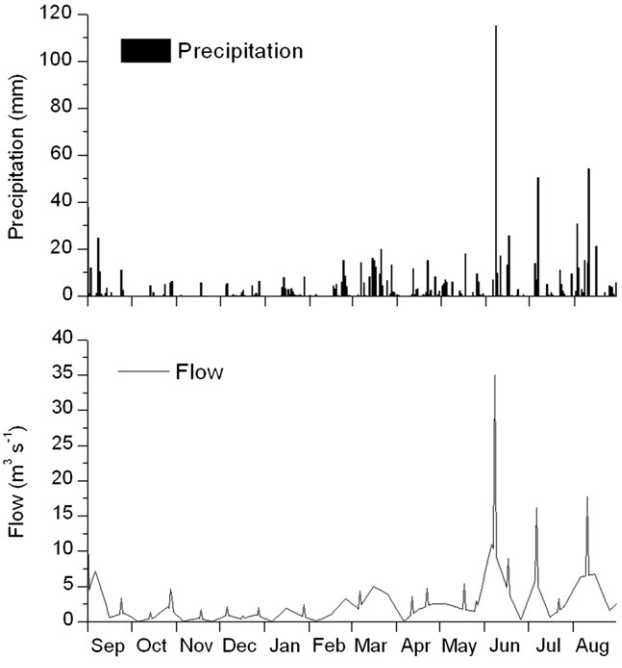

Fig. 4. Daily precipitation and modelled mean flows at R20 (outlet).

Table 4
Coefficients of depth and velocity in each segment as a function of flow (Eqs. (2a) and (2b)).

Segment no.	Velocity ($m\,s^{-1}$)		Depth (m)	
	Multiplier, a	Exponent, b	Multiplier, c	Exponent, d
R450	2.8427	0.2644	0.1600	0.4628
R500	1.6721	0.2702	0.1989	0.4783
R320	1.1931	0.2904	0.1761	0.5175
R410	1.1837	0.3057	0.1356	0.5388
R180	0.7311	0.3265	0.1352	0.5609
R20	0.5824	0.3528	0.0900	0.5807
R440	1.3738	0.2985	0.1375	0.5295
R50	1.0966	0.3173	0.1159	0.5520

Note: WASP requires input of velocity ($m\,s^{-1}$) and depth (m) to be a function of flow ($m^3\,s^{-1}$), Velocity = a $*Q^b$ and Depth = c $*Q^d$.

3. Results

3.1. Precipitation and flow

Fig. 4 shows the daily precipitation and modelled mean flow at one segment (R20) from September 2007 to August 2008. This figure clearly shows the typical seasonal variation. Most precipitation occurred in a limited number of storm events, especially in summer with precipitation at this time (June–August) accounting for 48% of total annual amount. This is very typical for the area, where rainfall is generally controlled by monsoon climate. During the winter season (Oct–Dec) flow dropped below 1 $m^3\,s^{-1}$ before increasing at the beginning in February. There were clearly three high flood events in summer months (June, July and August). The highest flow occurred in Jun. 8, 2008, reaching 35 $m^3\,s^{-1}$. In WASP, the user should input depth (m) and velocity ($m\,s^{-1}$) as a function of flow the equation coefficients are listed in Table 4 for each of the segments.

3.2. Suspended particles transport

Fig. 5 shows the results of modelled TSS along the main stream channel. The concentration of TSS decreases very quickly before stabilising between R410 and R20. TSS concentrations were significantly higher during the higher flow period compared to the lower flow period. The majority of particles were released during high flow events in summer. TSS concentration is known to increase with

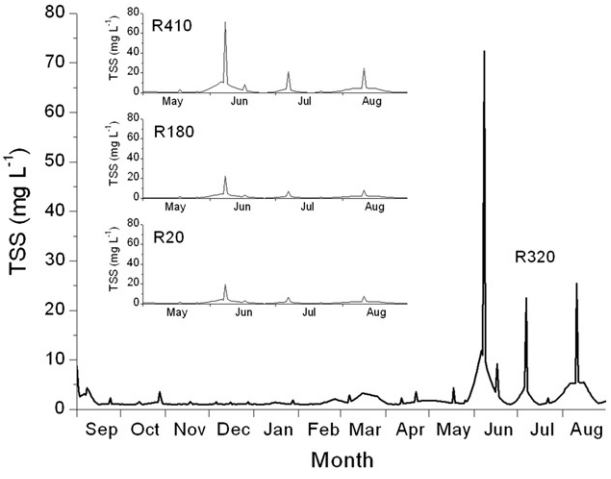

Fig. 5. Modelled results of TSS along the main stream channel (values in May–August for R410, R180, R20 are displayed).

Table 5
Comparison of modelled and observed TSS values.

Segment no.	TSS (mg L^{-1}) Sep. 4, 2007		Difference	TSS (mg L^{-1}) Aug. 8, 2008		Difference
	Modelled	Observed	%	Modelled	Observed	%
R320	1.74	1.7	2.35	4.27	4.4	2.95
R410	0.69	0.76	9.21	1.94	2.0	3.00
R180	0.56	0.44	27.3	2.15	2.2	2.27
R20	0.53	0.7	24.3	2.13	2.1	1.43
Error	0.11			0.08		
% Error	11			2.5		
Bias	−0.02			−0.05		

Note: errors are calculated for each individual segment by Eqs. (8a), (8b), and (8c).

increasing water flow, due to both soil erosion (from the river banks and the flood plain) and sediment re-suspension. The total amount of solids released annually through segments R320 was estimated to be 59 metric tons. Three high flow events in summer were identified (Fig. 4) to calculate the contribution of high flow events to particle transport. The three high flow dates were Jun. 8, 2008, Jul. 7, 2008 and Aug. 11, 2008. The total amount of solids released through R320 on the above three dates represented 23%, 5% and 6%, respectively of the annual total.

The modelled TSS concentrations were compared with the observed values (Lin et al., 2011) in Table 5. Eqs. (8a), (8b), and (8c) is used to evaluate the overall model performance. The results show that the average modelling error for the TSS of Sep. 4, 2007, is 0.11 mg L^{-1}, the relative error is 11%, and the bias is −0.02 mg L^{-1}. It has to be noted that the relative error increased when TSS concentration is as low as 0.5 mg L^{-1} (R180 and R20). At low concentrations, there will be bigger proportion of fine particles. This may cause the re-suspension and sedimentation of particles at different velocities. This may explain the increased relative errors for downstream segments at low flow. Similarly, for the TSS of Aug. 8, 2008, results show that the average modelling error is 0.08 mg L^{-1}, the relative error is 2.5%, and the bias is −0.05 mg L^{-1}.

3.3. Transport of Hg–THg, DHg and MeHg

Fig. 6 presents the modelled Hg concentration as a function of distance from a point source during September 2007 and August 2008 for THg, DHg and MeHg. The results are listed in Table 6. Eqs. (8a), (8b), and (8c) were used to evaluate the modelled results.

All Hg concentrations (THg, DHg and MeHg) decreased very rapidly along the stream. For example, THg concentration decreased to below 50 ng L^{-1}, 15 km away from the source (R500, 2100 ng L^{-1}). Sedimentation of TSS is an important factor in reducing Hg transport downstream. RHg was used in the modelling to simulate the concentrations of DHg and MeHg due to the fact that majority of THg exists in the form HgS (Lin et al., 2010). The Hg in HgS cannot take part in the adsorption process or methylation reactions. It is therefore better to use RHg in chemical equilibrium-based models for mining areas with high inactive Hg content (HgS). DHg concentration accounts less than 25% of THg concentration for most of samples; MeHg was also very low compared with THg. The model gave relatively reasonable results for THg, DHg and MeHg, with relative error <10%.

As described in the above section, the transport of suspended particles mainly happens during high flow events. An estimate of contribution of high flow to transport of THg is also needed. The discharge of Hg through a certain segment is calculated by Eq. (9):

$$Hg = [THg] \times Q \times T \times 10^{-9} \quad (9)$$

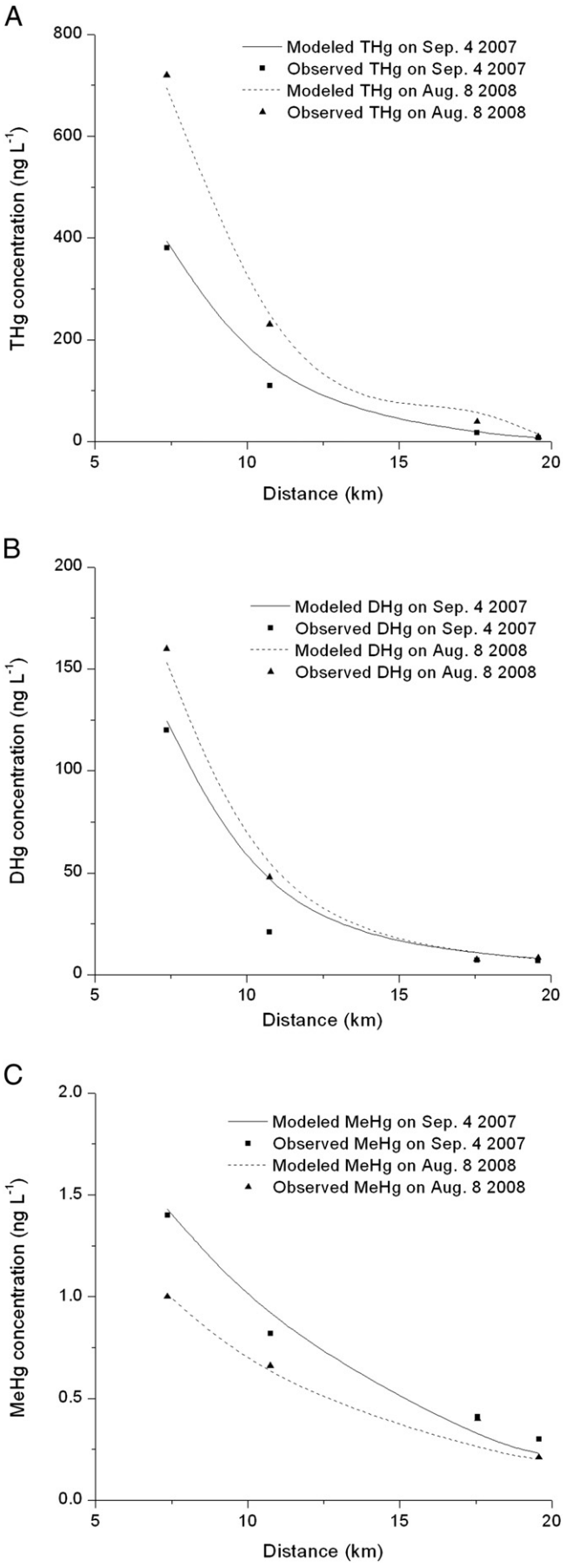

Fig. 6. Modelled and observed Hg concentrations for the two sampling campaigns: THg (A), DHg (B) and MeHg (C).

Table 6
Modelled Hg concentrations for THg, DHg and MeHg.

Hg species	Segment no.	Sep. 4, 2007			Aug. 8, 2008		
		Modelled	Observed	% Error	Modelled	Observed	% Error
THg (ng L^{-1})	R320	394	380	3.7	695	720	3.5
	R410	88	110	20.0	250	230	8.7
	R180	15	17	11.8	57	39	46.2
	R20	7.9	6.6	19.7	14	9.3	50.5
	Overall error	13			19		
	% Error	7.7			7.2		
	Bias	−2.2			5.4		
DHg (ng L^{-1})	R320	124.4	120	3.7	153.1	160	4.3
	R410	26.1	21	24.3	28.4	48	40.8
	R180	10	7.2	38.9	9.9	7.5	32.0
	R20	8.2	6.7	22.4	7.9	8.3	4.8
	Overall error	3.8			10		
	% Error	9.0			13		
	Bias	3.5			−6.1		
MeHg (ng L^{-1})	R320	1.43	1.4	2.1	1.01	1	1.0
	R410	0.85	0.82	3.7	0.57	0.66	13.6
	R180	0.3	0.41	26.8	0.25	0.4	37.5
	R20	0.23	0.3	23.3	0.22	0.21	4.8
	Overall error	0.07			0.09		
	% Error	7.4			11		
	Bias	−0.04			−0.06		

Note: errors are calculated for each individual segment by Eqs. (8a), (8b), and (8c).

where

Hg is total discharge of Hg (kg);
[THg] is the THg concentration at a certain segment (ng L^{-1});
Q is the flow at a certain segment (m^3 s^{-1});
T is the time period over which the calculation is carried out, in the present study performed daily, so T = 86,400 s day^{-1}.

The annual total discharge of Hg through R320 was 8.8 kg Hg, while total discharge of Hg through R20 was 2.6 kg Hg. Fig. 8 illustrate the estimated Hg mass balance for Xiaxi. The result indicates that about 70% of Hg was retained in the stream through sedimentation. The contribution of the three high-flow events described above was significant. The discharge of THg during these events accounts for 37%, 6% and 8% of total annual discharge of Hg at R20, indicating that they were responsible for about 50% of THg downstream of this point.

4. Discussion

Higher flows usually carry more suspended solids and the TSS followed a similar trend to the flow values. Good linear correlation was found between TSS and flow. Calcine tailings act as the main sources of particles and THg to system. The high flow events also led to a considerable release of suspended particles. The three high flow events accounts for more than 30% of annual release. Uncertainty assessment was carried out to assess the impacts of flow on TSS within the 95% confidential interval. Eqs. (8a), (8b), and (8c) were used to assess the range of errors within the 95% confidential interval. Results showed that the bias of simulated results was between −0.14–0.10 mg L^{-1} for Sep. 4, 2007 and −0.42–0.31 mg L^{-1} for Aug. 8, 2008. The relative errors for the lower and upper ranges are between −18.2–16.8% for Sep 4, 2007, and −15.7–11.8% for Aug. 8, 2008. Results indicate that there are little uncertainties in the flow and TSS correlation due to better fitting of linear regression.

THg, DHg and MeHg concentrations were modelled and compared to measured values during two flow regimes, with relative errors typically around 10%. The modelled THg results downstream usually gave higher concentrations, especially for data on Aug. 8, 2008, perhaps caused by enhanced Hg0 evasion under higher temperature in summer. Due to lack of the required data, the reduction and evasion of Hg was not included in the modelling. Thus subsequent work may focus on obtaining the water–air exchange fluxes in order to improve the model. Modelled MeHg results gave lower concentrations than those observed downstream (R180&R20), indicating that there might be enhanced methylation or additional MeHg sources unaccounted for in the downstream areas. A more detailed survey should be conducted in order to identify areas where methylation occurs, for example the contribution from rice paddy fields (Zhang et al., 2010b). If quantified properly, different M/D can then be assigned to these river segments.

Uncertainty assessment was carried out to assess the impacts of flow on THg as described in 2.3.6. Fig. 7 shows the simulated results of THg at upper and lower range of linear regression equations for Sep. 4, 2007 and Aug. 8, 2008. Eqs. (8a), (8b), and (8c) were used to assess the range of errors within the 95% confidential interval. Results showed that the bias of simulated results was between −110–112 ng L^{-1} for Sep. 4, 2007 and −211–243 ng L^{-1} for Aug. 8, 2008. The relative errors for the lower and upper ranges are between −86–88% for Sep 4, 2007, and −84–97% for Aug. 8, 2008. This shows that the modelling is very sensitive to boundary conditions generated by the flow and THg relationship. It is therefore important to obtain more knowledge of the flow and THg so that the range of regression equations can be narrowed resulting in smaller error ranges.

High flow events are the main contributors for particle release and Hg discharge. The annual total discharge of Hg through R320 was 8.8 kg Hg, while total discharge of Hg through R20 was 2.6 kg Hg. The contribution of the three high-flow events accounted for about 50% of THg discharged at R20. This means that about 70% of Hg is retained in the stream through sedimentation during the modelling period (from Sep 1, 2007 to Aug 31, 2008). Suchanek et al. (2009) estimated the discharge of Hg from Clear Lake to Cache Creek was 2.8 kg Hg $year^{-1}$ at Sulphur Bank Mercury Mine Area, USA which is similar to the present study. Work conducted at the St. Lawrence River, Canada estimated that Hg discharge was 1180 kg Hg $year^{-1}$ (73% as particulate) (Quemerais et al., 1999). The St. Lawrence River is much larger than both the present study site and that of Cache Creek. The transport of sediments and Hg is therefore, also much greater. However, all studies confirmed that particles were an important pathway for Hg transport. A big fraction of the Hg in stream water and sediments exists as grains of inert cinnabar (HgS). This fraction is not available for adsorption/desorption equilibrium reactions as is assumed by the WASP model. Using THg as input to the model therefore causes overestimation of DHg and MeHg

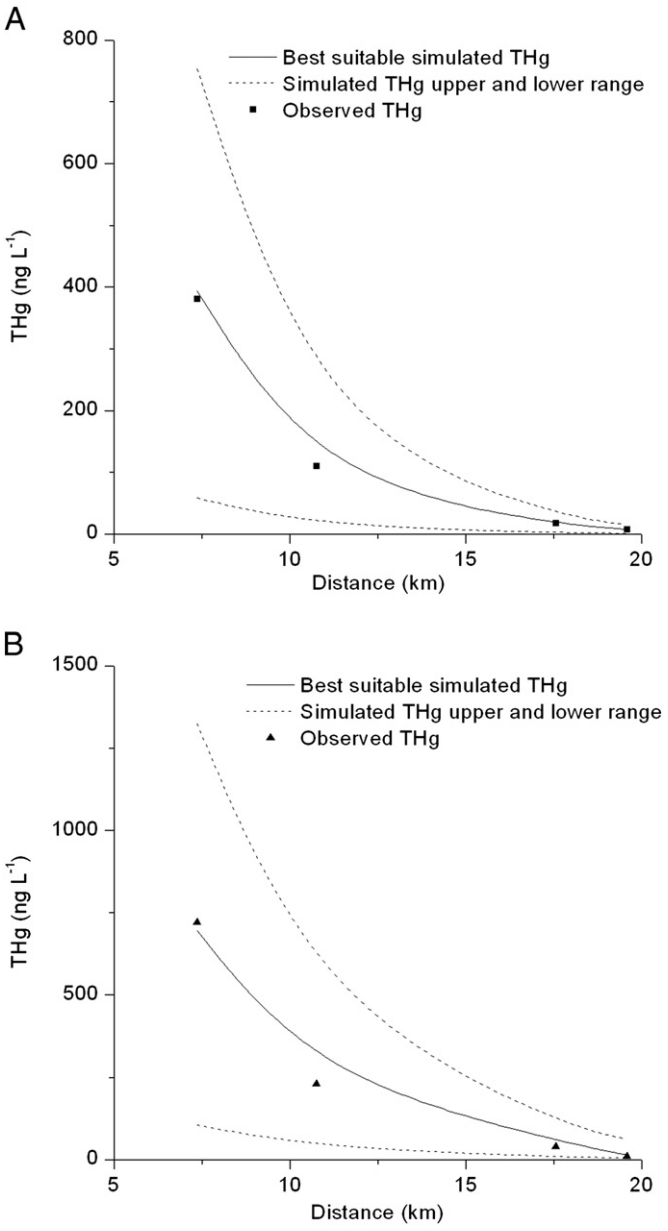

Fig. 7. Sensitivity analysis on THg concentrations for the two sampling campaigns: Sep. 4, 2007 (A) and Aug. 8, 2008 (B). The upper and lower dashed lines are generated from upper and lower range of rating curve under 95% confidential interval shown in Fig 3b.

concentrations. Instead, RHg is found to be an appropriate model input. Particle concentrations and particle behaviour related to flow conditions are critical for this modelling effort; thus, better understanding and more intense monitoring of TSS values are needed.

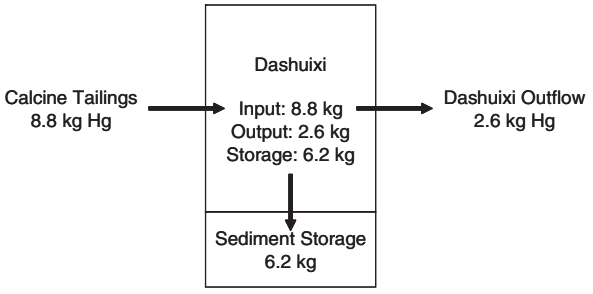

Fig. 8. Estimated Hg mass balance for Xiaxi River (kg yr^{-1}).

Table 7
Summary of sensitivity analysis results for various parameters.

Input variable	Range of input variable	Output variable	Range of errors (%)
K_d	10^2–10^6 (coarse) 10^6–10^8 (fine)	DHg	−39–33
M/D	10^{-5}–1	MeHg	−20–28
Rating curve for flow versus TSS	95% confidential interval for regression	TSS loading	−18–17
Rating curve for flow versus THg	95% confidential interval for regression	THg loading	−86–97
Flow	±10%	THg	−11–11

Note: K_d stands for partitioning coefficient of Hg on particles; M/D stands for methylation and demethylation ratio.

Since the rating curves for TSS and THg are derived based on flow, it is important to test the impact of fluctuation of flow on final results. It is done by testing simulated results by changing flow with ±10% difference. The relative error generated was also around ±10% due to the linear correlation with what was used in deriving the rating curves for TSS and THg. Table 7 summarises the results of sensitivity analysis for various parameters.

5. Conclusions

A method was developed to simulate the Hg transport at places where there exists no routine hydrological monitoring. The GIS based hydrological model HEC-HMS was applied to simulate fluctuations in stream flow based on publicly available precipitation data. This method addresses the problem of a lack of flow data as an input to transport and fractionation models. The hydrological model was coupled with the Hg transport and fractionation models WASP in order to predict Hg transport and concentrations at different parts of the river at different flow regimes. The model produces reasonable simulation results for TSS, THg, DHg and MeHg, with relative errors generally around 10% for the modelled parameters. High flow events are the main contributors for release of both suspended particles and Hg. The three high flow events account for about 50% of annual discharge of THg. The annual total discharge of Hg was 8.8 kg Hg high up in the stream and 2.6 kg where the stream meets a large river 20 km downstream of the pollution source. Hence, about 70% of Hg is retained in the stream through sedimentation.

Acknowledgment

We greatly acknowledge the in depth comments and detailed suggestions from four anonymous reviewers.

References

Allison JD, Allison TL. Partition coefficients for metals in surface water soil and waste. Athens, GA: U.S. Environmental Protection Agency; 2005. EPA/600/R-05/074.
Ambrose RB, Wool TA, Connolly JP, Schanz RW. WASP4, a hydrodynamic and water quality model—model theory, user's manual, and programmer's guide. Athens, GA: U.S. Environmental Protection Agency; 1988. EPA/600/3-87-039.
Anderson ML, Chen ZQ, Kavvas ML, Feldman A. Coupling HEC-HMS with atmospheric models for prediction of watershed runoff. J Hydrol Eng 2002;7:312–8.
Berzas Nevado JJ, Garcia Bermejo LF, Rodriguez Martin-Doimeadios RC. Distribution of mercury in the aquatic environment at Almadén, Spain. Environ Pollut 2003;122: 261–71.
Bravo R, Dow DA, Rogers JR. Parameter determination for the Muskingum-Cunge flood routing method. Water Resour Bull 1994;30:891–9.
Carroll RWH, Warwick JJ, Heim KJ, Bonzongo JC, Miller JR, Lyons WB. Simulation of mercury transport and fate in the Carson River, Nevada. Ecol Modell 2000;125: 255–78.
Feng X, Qiu G. Mercury pollution in Guizhou, Southwestern China — an overview. Sci Total Environ 2008;400:227–37.
Gill GA, Bruland KW. Mercury speciation in surface freshwater systems in California and other areas. Environ Sci Technol 1990;24:1392–400.
Hines ME, Horvat M, Faganeli J, Bonzongod JC, Barkaye T, Majorf EB, et al. Mercury biogeochemistry in the Idrija Stream, Slovenia, from above the Mine into the Gulf of Trieste. Environ Res 2000;83:129–39.

Horvat M, Nolde N, Fajon V, Jereb V, Logar M, Lojen S, et al. Total mercury, methylmercury and selenium in mercury polluted areas in the province Guizhou, China. Sci Total Environ 2003;304:231–56.
Knightes CD, Sunderland EM, Barber MC, Johnston JM, Ambrose RB. Application of ecosystem-scale fate and bioaccumulation models to predict fish mercury response times to changes in atmospheric deposition. Environ Toxicol Chem 2009;28:881–93.
Lin Y, Larssen T, Vogt RD, Feng XB. Identification of fractions of mercury in water, soil and sediment from a typical Hg mining area in Wanshan, Guizhou province, China. Appl Geochem 2010;25:60–8.
Lin Y, Larssen T, Voft RD, Feng XB, Zhang H. Transport and fate of mercury under different hydrologic regimes in polluted stream in mining area. J Environ Sci 2011;23:757–64.
Matilainen T. Involvement of bacteria in methyl-mercury formation in anaerobic lake waters. Water Air Soil Pollut 1995;80:757–64.
Oremland RS, Miller LG, Dowdle P, Connell T, Barkay T. Methyl-mercury oxidative degradation potentials in contaminated and pristine sediments of the Carson River, Nevada. Appl Environ Microbiol 1995;61:2745–53.
Qiu GL, Feng XB, Wang SF, Shang LH. Mercury and methylmercury in riparian soil, sediments, mine-waste calcines, and moss from abandoned Hg mines in east Guizhou province, southwestern China. Appl Geochem 2005;20:627–38.
Qiu GL, Feng XB, Wang SF, Fu XW, Shang LH. Mercury distribution and speciation in water and fish from abandoned Hg mines in Wanshan, Guizhou province, China. Sci Total Environ 2009;407:5162–8.
Quemerais B, Cossa D, Rondeau B, Pham TT, Gagnon P, Fortin B. Sources and fluxes of mercury in the St. Lawrence river. Environ Sci Technol 1999;33:840–9.
Suchanek TH, Cooke J, Keller K, Jorgensen S, Richerson PJ, Eagles-Smith CA, Harner EJ, Adam DP. A mass balance mercury budget for a mine-dominated lake: Clear Lake, California. Water Air Soil Pollut 2009;196:51–73.
Ullrich SM, Tanton TW, Abdrashitova SA. Mercury in the aquatic environment: a review of factors affecting methylation. Crit Rev Environ Sci Technol 2001;31:241–93.
United States Department of Agriculture (USDA). Urban hydrology for small watersheds. Technical Release, 55 (TR-55). ; 1986.
van Rijin LC. Sediment transport, part II: suspended load transport. J Hydraul Eng 1984;110:1613–41.
Watras CJ, Bloom NS, Claas SA, Morrison KA, Gilmour CC, Craig SR. Methyl-mercury production in the anoxic hypolimnion of a dimictic seepage lake. Water Air Soil Pollut 1995a;80:735–45.
Watras CJ, Morrison KA, Host JS, Bloom NS. Concentration of mercury species in relationship to other site-specific factors in the surface waters of northern Wisconsin lakes. Limnol Oceanogr 1995b;40:556–65.
Xun L, Campbell NER, Rudd JWM. Measurements of specific rates of net methyl-mercury production in the water column and surface sediments of acidified and circumneutral lakes. Can J Fish Aquat Sci 1987;44:750–7.
Yusop Z, Chan CH, Katimon A. Runoff characteristics and application of HEC-HMS for modelling stormflow hydrograph in an oil palm catchment. Water Sci Technol 2007;56:41–8.
Zagar D, Knap A, Warwick JJ, Rajar R, Horvat M, Cetina M. Modelling of mercury transport and transformation processes in the Idrijca and Soca river system. Sci Total Environ 2006;368:149–63.
Zhang H, Feng X, Larssen T, Shang L, Vogt RD, Rothenberg SE, et al. Fractionation, distribution and transport of mercury in rivers and tributaries around Wanshan Hg mining district, Guizhou province, southwestern China: part 1—total mercury. Appl Geochem 2010a;25:633–41.
Zhang H, Feng X, Larssen T, Shang L, Vogt RD, Rothenberg SE, et al. Fractionation, distribution and transport of mercury in rivers and tributaries around Wanshan Hg mining district, Guizhou province, southwestern China: part 2—methyl mercury. Appl Geochem 2010b;25:642–9.